Proc. Natl. Acad. Sci. USA
Vol. 90, pp. 11341–11345, December 1993
Biophysics

Elastic free energy of anisotropic helical ribbons as metastable intermediates in the crystallization of cholesterol

(membrane/chirality/lecithin/bile/gallstone)

DOO SOO CHUNG†, GEORGE B. BENEDEK†, FRED M. KONIKOFF‡§, AND JOANNE M. DONOVAN‡¶

†Department of Physics and Center for Materials Science and Engineering, Massachusetts Institute of Technology, Cambridge, MA 02139; ‡Department of Medicine, Harvard Medical School, Brigham and Women's Hospital, Boston, MA 02115; and ¶Brockton/West Roxbury Veterans Affairs Medical Center, West Roxbury, MA 02132

Contributed by George B. Benedek, August 18, 1993

ABSTRACT **We report measurements of the geometrical structure and temporal evolution of metastable helical intermediates in the pathway for cholesterol crystallization in native and model biles. We find that the lecithin component in the bile can dramatically affect the kinetics along this pathway. We also present a theoretical description of these helical intermediates using an elastic free energy appropriate for anisotropic bilayers of tilted chiral amphiphiles, which provides a quantitative description of the observed helical ribbon geometry and insight into the relative free energies of the observed metastable intermediates.**

Cholesterol gallstone disease is consequent upon the formation of cholesterol monohydrate crystals (ChMs) after supersaturation of bile in the gallbladder (1). We have recently demonstrated (2) that cholesterol crystallization involves a succession of metastable intermediate structures: filaments → helical ribbons → tubules, and thence to ChMs, the thermodynamically stable crystal habit (3). In view of the clinical importance of controlling cholesterol crystallization, we have carried out experimental and theoretical studies of kinetics and energetics of these metastable intermediates in a series of model biles. Although, to our knowledge, helical ribbon structures had not been previously reported in bile, twisted strips, helical ropes, helical ribbons, and tubules have been observed in a variety of systems composed of chiral amphiphiles (4–9). To understand the extraordinary helical and tubular superstructures formed in bile, we shall adopt and extend previous theoretical models for the elastic free energy of bilayers whose symmetry is broken by the chirality. In Fig. 1*a* we show the geometrical quantities required to describe a right-handed helical ribbon surface. The coordinates of a point Y on this surface are

$$(\rho \cos \phi,\ \rho \sin \phi,\ \rho\phi \tan \psi + h),\ 0 \le h \le w/\cos \psi, \quad [1]$$

where ρ, w, ψ, ϕ, and h are, respectively, the radius, width, pitch angle, azimuthal angle, and distance from the edge as shown. In 1986, Helfrich (10) proposed a simple elastic model in which the optimal shape of a helical ribbon is controlled by a balance between bending of the ribbon and torsion of its edges, leading to a universal pitch angle of 45° for an elastically isotropic ribbon. Two years later Helfrich and Prost (11) generalized the bending free energy for anisotropic bilayers. To account for the lack of mirror reflection symmetry of bilayers of chiral molecules, they also added a term linear in the surface curvature to the elastic free energy (11). Despite these refinements, the analysis of the pitch angle was made only for an isotropic bilayer and the pitch angle remained 45°. In 1990, Ou-Yang and Liu (12) modeled the helical ribbon as a cholesteric liquid crystal layer and also obtained the pitch angle of 45°.

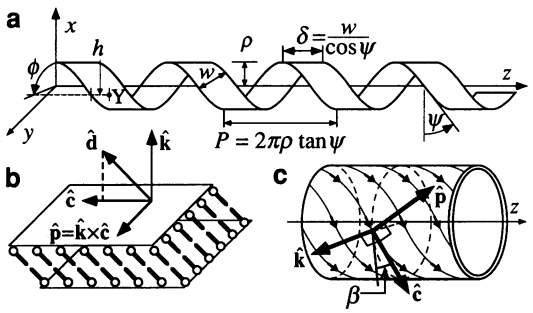

FIG. 1. (*a*) Geometry of a helical ribbon. ρ, Radius; ψ, pitch angle; P, pitch; w, width; δ, width along the z axis. (*b*) Local coordinate system of a symmetric tilted bilayer. (*c*) Local coordinate system on a tubule made of a tilted bilayer. Helical lines with arrows show the direction of $\hat{\mathbf{c}}$.

Herein, we describe experimentally observed helical ribbon structures with either of two distinctive pitch angles: 54° or 11°. We also present a form for the elastic free energy of anisotropic chiral bilayers that provides analytical expressions for the geometrical features and growth of the helical ribbon structures observed in our biles.

MATERIALS AND METHODS

All model biles were composed of the common bile salt sodium taurocholate, lecithin, and cholesterol in a molar ratio of 97.5:0.8:1.7. Sodium taurocholate (Sigma) was recrystallized and found to be >98% pure by HPLC and TLC. Cholesterol (Nu Chek Prep, Elysian, MN) was >99% pure by TLC, GC, and HPLC. Grade I egg yolk lecithin (Lipid Products, Nutley, U.K.) was >99% pure by TLC. Synthetic *sn*-1-16:0-*sn*-2-18:1 lecithin (lecithin I) and *sn*-1-16:0-*sn*-2-16:0 lecithin (lecithin II) were obtained from Avanti Polar Lipids. Model biles *A*, *B*, *C*, and *D* contained lecithin I, a 1:1 mixture of lecithin I and lecithin II, egg yolk lecithin, and lecithin II, respectively. Native bile was a generous gift from M. Cahalane (Beth Israel Hospital, Boston) (2). Using TLC, no degradation of the components of bile was observed during our experiments.

At a total lipid concentration of 70 mg/ml (0.15 M NaCl/3 mM NaN_3), all four model biles formed micellar solutions with a mean hydrodynamic radius of 17 ± 5 Å (2, 13). Meticulous precautions were taken to reduce the nucleating effect of dust. A 5-ml vial with a Teflon septum cap was acid-cleaned, rinsed, filled with Milli-Q water (Millipore),

The publication costs of this article were defrayed in part by page charge payment. This article must therefore be hereby marked "*advertisement*" in accordance with 18 U.S.C. §1734 solely to indicate this fact.

Abbreviation: ChM, cholesterol monohydrate crystal.

§Present address: Department of Gastroenterology, Ichilov Hospital, Tel-Aviv Medical Center, Tel-Aviv, Israel.

dried by purging clean argon gas using needles through the septum, and sealed. After incubation for 1 h at 60°C, 500 μl of bile and 2500 μl of saline solution were injected into the vial through a 0.22-μm (pore size) filter and incubated at 37°C. At intervals, 150-μl samples were transferred to a sealed drop-slide on a temperature-controlled stage (37°C) for a microscope (Optiphoto-Pol, Nikon). Images were taken with a video camera and digitized with a frame grabber on an Apple Macintosh IIci computer. Public-domain IMAGE software (National Institutes of Health) was used for image enhancement and measurement of the diameter, pitch, and width of helical ribbons. Measured values of pitch and width were corrected for the inclination of the helical ribbon axis from the observing plane. Handedness of helices was determined by comparing the relative vertical height of different parts of the ribbon. Pitch angles ψ were calculated from the ratio of the pitch to the radius (see Fig. 1*a*). The reported uncertainty in ψ represents the 90% confidence interval.

RESULTS

Micellar model biles initially prepared were thermodynamically stable with a cholesterol saturation index of about 90% (2, 13). Because of the location of the phase boundary in the pseudo-quaternary phase diagram, a 1:6 dilution of bile resulted in cholesterol-supersaturated bile (cholesterol saturation index > 200%) containing both mixed micelles and vesicles (2, 13). Within 2–4 h of dilution, filamentous structures were observed that appear to be composed of anhydrous cholesterol (2). Within a few days, in model biles *A*, *B*, and *C*, filaments coexisted with helices, tubules, and plate-like crystals, and eventually, only plate-like ChMs remained. A particularly striking finding was that in model bile *D* composed with lecithin II alone, no helical structures were observed to form over a 2-week period. Initial helical ribbon structures had high pitch angles (≈54°), as shown in Fig. 2*a*, and grew laterally while maintaining a fixed pitch angle to form tubules, as shown in Fig. 2*b*. Within a few weeks, high pitch helices disappeared, while helices with low pitch angle (≈11°) formed independently and followed a similar growth pattern (see Fig. 2 *c* and *d*). Due to Brownian motion and convection, it is difficult to track a single helix over many days. Nevertheless, we directly observed the dissolution of two high pitch helices and numerous other transitions described in Fig. 3. In contrast, we never found a direct conversion from high to low pitch helices. Tubules grown from low pitch helices were sometimes observed to fracture, producing plate-like ChMs. Such a fracture was found even in native bile as shown in Fig. 2 *e* and *f*. Without exception, all helical structures, including tubules with residual helical marks, were right-handed. Fig. 3 summarizes the sequence and relative stability of the intermediate structures discussed above.

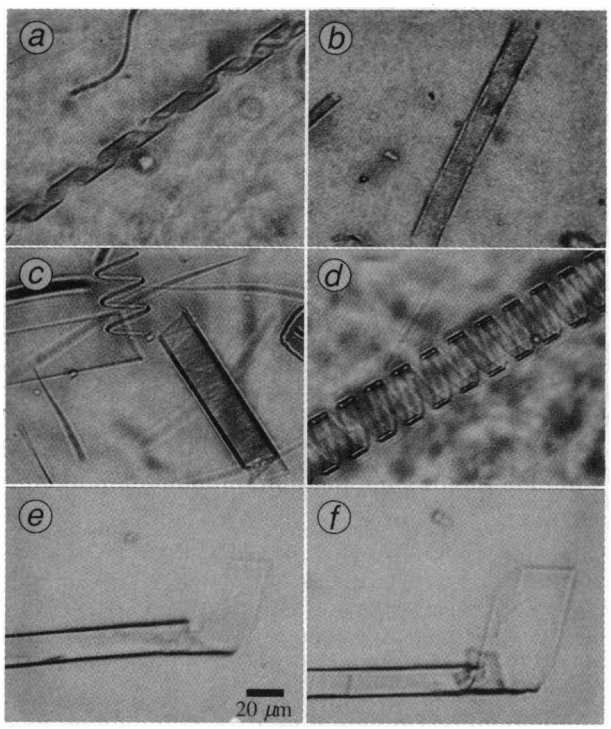

FIG. 2. Typical helical and tubular structures in bile. (*a* and *b*) High pitch helical ribbon and helically grown tubule, respectively. (*c* and *d*) Similar structures of low pitch. The tubule in *c* shows helical marks of low pitch. (*e*) Fracture of a low pitch tubule. (*f*) Subsequent growth of the low pitch tubule in *e* into a plate-like ChM after 12 h. (Bar = 20 μm.)

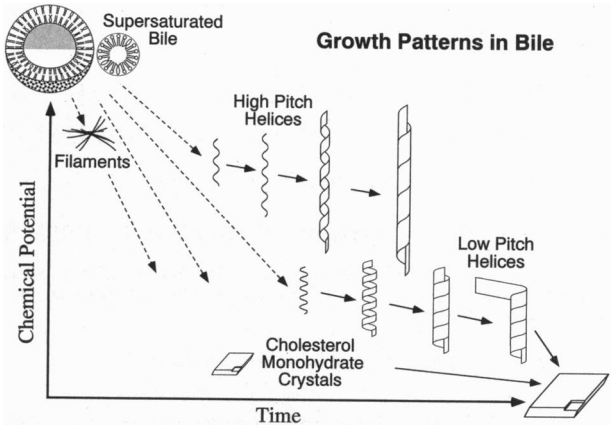

FIG. 3. Sequence and relative stability of metastable intermediates plotted as functions of time after supersaturation of bile. Less-stable structures have higher chemical potential. Solid and dotted arrows represent, respectively, observed and presumed transitions.

Fig. 4 displays measurements of pitch as a function of diameter of representative helical ribbons in model bile *A*. After 1 day of incubation, high pitch helices with diameters of 3–15 μm were observed (Fig. 4*a*). However, after 10 days, only low pitch helices remained (Fig. 4*b*). The diameters of the low pitch helices were generally larger than those of the high pitch helices. The solid lines in Fig. 4 depict linear least square fits of pitch versus diameter for the high and low pitch helices. Pitch angles ψ as calculated from the slopes were 54.3 ± 2.3° and 11.1 ± 0.5°. In model bile *B*, filaments and high and low pitch helices formed in the same sequence, but more slowly. Fig. 5 displays the population distribution of high and low pitch helices found in model bile *B* as a function of time. Initially, high pitch helices predominated and gradually grew in ribbon width, but over time the population of independently formed low pitch helices increased. Pitch angles for the helices in model bile *B* were 54.1 ± 0.8° and 11.5 ± 0.7°,

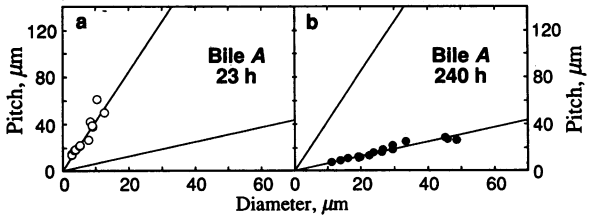

FIG. 4. Pitch versus diameter of helices in model bile *A* observed at the indicated times after supersaturation. Pitch angles were 54.3 ± 2.3° and 11.1 ± 0.5°.

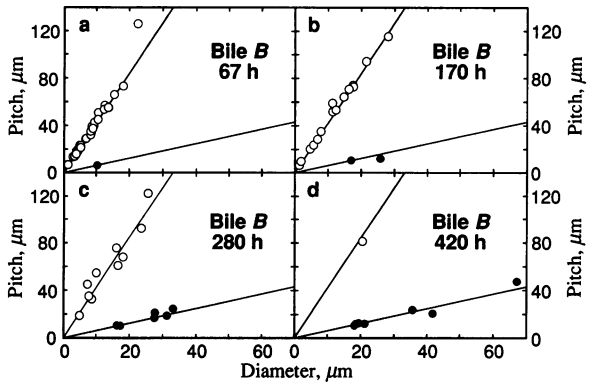

FIG. 5. Pitch versus diameter of helices in model bile *B* observed at various times after supersaturation. Pitch angles were 54.1 ± 0.8° and 11.5 ± 0.7° for high (○) and low (●) pitch helices, respectively.

within experimental error of values for model bile *A*. In model bile *C*, the structure and time sequence of the intermediates were quite similar to model bile *A*.

Fig. 6 displays all the data for biles *A*, *B*, and *C*. Regardless of diameter, all helices have pitch angles of either $\psi = 53.7 \pm 0.8°$ or $\psi = 11.1 \pm 0.5°$, in sharp contrast to the prediction for isotropic bilayers shown as the dotted line in Fig. 6.

DISCUSSION

Theory for the Shape of Helical Ribbons. Let us model the helical ribbon drawn in Fig. 1*a* as constituted of *n* symmetric bilayers of tilted chiral amphiphiles that have the same local structure as chiral tilted smectic layers. Since observed helices have well-defined macroscopic shapes, we infer that bilayer molecules have long-range positional and orientational order. The configuration of a bilayer in the ribbon can be described using a local coordinate system (see Fig. 1*b*) determined by the two unit vectors $\hat{\mathbf{k}}$ and $\hat{\mathbf{c}}$, which lie along the direction normal to the ribbon plane and along the projection of the molecular tilt, $\hat{\mathbf{d}}$, onto the ribbon plane, respectively. The third axis, $\hat{\mathbf{k}} \times \hat{\mathbf{c}}$, is denoted as $\hat{\mathbf{p}}$. The elastic free energy associated with a small deformation of chiral smectic phases has been derived by de Gennes (14) in terms of the rotation of the local frame of reference around the space axes. Dahl and Lagerwall (15) provided a translation table from the spatial derivatives of rotations of the local frame of reference to a vector calculus representation with $\hat{\mathbf{k}}$, $\hat{\mathbf{c}}$, and $\hat{\mathbf{p}}$. Using Dahl and Lagerwall's reformulation (15), we express the elastic free energy per unit area of the ribbon as

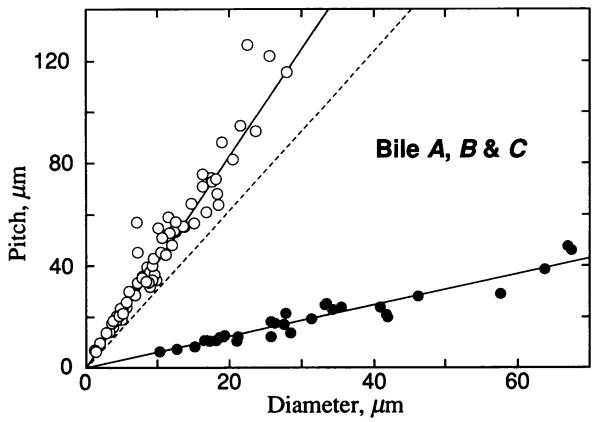

FIG. 6. Pitch versus diameter of helices in model biles *A*, *B*, and *C* combined. Pitch angles were 53.7 ± 0.8° and 11.1 ± 0.5° for high (○) and low (●) pitch helices, respectively. The dotted line represents the pitch angle of 45°.

$$G_{\text{bilayer}} = G_k + G_c + G_{kc} + G_{\text{chiral}}, \quad [2]$$

where

$$G_k = \frac{A_{11}}{2}[\hat{\mathbf{c}}\cdot(\nabla\hat{\mathbf{k}})\cdot\hat{\mathbf{p}}]^2 + \frac{A_{12}}{2}[\hat{\mathbf{c}}\cdot(\nabla\hat{\mathbf{k}})\cdot\hat{\mathbf{c}}]^2 + \frac{A_{21}}{2}[\hat{\mathbf{p}}\cdot(\nabla\hat{\mathbf{k}})\cdot\hat{\mathbf{p}}]^2,$$

$$G_c = \frac{B_1}{2}[\hat{\mathbf{k}}\cdot(\nabla\times\hat{\mathbf{c}})]^2 + \frac{B_2}{2}(\nabla\cdot\hat{\mathbf{c}})^2 + \frac{B_3}{2}\{\hat{\mathbf{c}}\cdot[\nabla\times\hat{\mathbf{c}} + (\nabla\hat{\mathbf{k}})\cdot\hat{\mathbf{p}}]\}^2$$

$$- B_{13}[\hat{\mathbf{k}}\cdot(\nabla\times\hat{\mathbf{c}})]\{\hat{\mathbf{c}}\cdot[\nabla\times\hat{\mathbf{c}} + (\nabla\hat{\mathbf{k}})\cdot\hat{\mathbf{p}}]\},$$

$$G_{kc} = -C_1[\hat{\mathbf{c}}\cdot(\nabla\hat{\mathbf{k}})\cdot\hat{\mathbf{p}}][\hat{\mathbf{k}}\cdot(\nabla\times\hat{\mathbf{c}})] - C_2[\hat{\mathbf{p}}\cdot(\nabla\hat{\mathbf{k}})\cdot\hat{\mathbf{p}}](\nabla\cdot\hat{\mathbf{c}}),$$

$$G_{\text{chiral}} = D_1\hat{\mathbf{k}}\cdot(\nabla\times\hat{\mathbf{c}}) - D_2\hat{\mathbf{c}}\cdot(\nabla\hat{\mathbf{k}})\cdot\hat{\mathbf{p}} - D\hat{\mathbf{c}}\cdot[\nabla\times\hat{\mathbf{c}} + (\nabla\hat{\mathbf{k}})\cdot\hat{\mathbf{p}}]. \quad [3]$$

Note that the elastic moduli in Eq. 3 correspond to the moduli in de Gennes' expression (14) integrated over the ribbon thickness. Thus our elastic moduli of the ribbon are determined both by the molecular configuration and by the number of constituent bilayers in the ribbon (16, 17). Here we have considered only "soft" deformations (15) of the layer shape and the molecular tilt direction $\hat{\mathbf{c}}$. G_k, the free energy per unit area associated with deformation of layer shape, contains only quadratic terms in $\nabla\hat{\mathbf{k}}$. The G_c term is associated with distortions of the directions of $\hat{\mathbf{c}}$ within the layer of a given shape and contains quadratic combinations of $\nabla\times\hat{\mathbf{c}}$ and $\nabla\cdot\hat{\mathbf{c}}$. The coupling of these two deformations of $\hat{\mathbf{k}}$ and $\hat{\mathbf{c}}$ is contained in the G_{kc} term. G_{chiral} contains three terms linear in $\nabla\hat{\mathbf{k}}$ or $\nabla\times\hat{\mathbf{c}}$ that change sign on mirror reflection through the $\hat{\mathbf{k}}\hat{\mathbf{c}}$ plane. These terms are allowed because of the lack of mirror reflection symmetry of the chiral molecules. Furthermore, their linearity implies an important contribution to the total elastic free energy G_{bilayer}.

It is instructive to calculate first the elastic free energy for a long hollow tubule that has the same structure as a helical ribbon but lacks the edges of the ribbon. For simplicity, we assume that variations of molecular arrangement from bilayer to bilayer are negligible and we treat a multilamellar ribbon as a single-bilayer ribbon with elastic moduli being a function of the number (*n*) of the constituent bilayers. Then, in cylindrical coordinates (ρ, ϕ, z), the unit vectors $\hat{\mathbf{k}}$, $\hat{\mathbf{c}}$, and $\hat{\mathbf{p}}$ of the tubule are given by (see Fig. 1*c*)

$$\hat{\mathbf{k}} = \hat{\boldsymbol{\rho}}, \quad \hat{\mathbf{c}} = \cos\beta\,\hat{\boldsymbol{\phi}} + \sin\beta\,\hat{\mathbf{z}}, \quad \hat{\mathbf{p}} = -\sin\beta\,\hat{\boldsymbol{\phi}} + \cos\beta\,\hat{\mathbf{z}}, \quad [4]$$

where β is the molecular phase angle (15) between $\hat{\mathbf{c}}$ and $\hat{\boldsymbol{\phi}}$. Substituting Eq. 4 into Eq. 3 and making notational substitutions, $K_n^{cc} = A_{12}$, $K_n^{pp} = A_{21}$, $K_n^{cp} = A_{11}/2$, and $K_n^* = -D_2$, where the subscript *n* denotes the dependence on the number of bilayers, we obtain an elastic free energy per unit area of a tubule similar to that of Helfrich and Prost (11),

$$G_{\text{tubule}}(\rho, \beta) = \frac{K_n^{cc}\cos^4\beta + K_n^{pp}\sin^4\beta + (K_n^{cp}/2)\sin^2 2\beta}{2\rho^2} - \frac{K_n^*\sin 2\beta}{2\rho}. \quad [5]$$

The K_n^{cc} and K_n^{pp} terms correspond to the bending of the bilayer along the $\hat{\mathbf{c}}$ and $\hat{\mathbf{p}}$ directions, respectively. The K_n^{cp} and K_n^* terms correspond to the twist of the coordinate system about the $\hat{\mathbf{k}}$ direction. The K_n^* term is present since the system has chirality. A positive value of K_n^* corresponds to a right-handed structure. Optimal geometry of the tubule is found by minimizing the free energy using the conditions,

$$\frac{\partial G_{\text{tubule}}}{\partial\rho} = \frac{\partial G_{\text{tubule}}}{\partial\beta} = 0. \quad [6]$$

These yield the following two equations for ρ and β, regarding the four elastic moduli as constants,

$$\rho K_n^* = K_n^{cc}\cos^3\beta \csc\beta + K_n^{pp}\sin^3\beta \sec\beta + K_n^{cp}\sin 2\beta, \quad [7]$$

$$\rho K_n^* = -K_n^{cc}\cos^2\beta \tan 2\beta + K_n^{pp}\sin^2\beta \tan 2\beta + K_n^{cp}\sin 2\beta. \quad [8]$$

By equating Eqs. 7 and 8, we find the remarkable result that the optimal molecular phase angle β is independent of the elastic moduli K_n^{cp} and K_n^* and is determined entirely by the ratio of two elastic moduli as

$$\tan^4\beta = K_n^{cc}/K_n^{pp}. \quad [9]$$

Substitution of Eq. 9 into Eq. 7 yields the optimal radius of the tubule,

$$\rho_n^{\text{tubule}} = 2(\overline{K}_n/K_n^*)\sin 2\beta, \quad [10]$$

where $\overline{K}_n \equiv (K_n^{cp} + \sqrt{K_n^{cc}K_n^{pp}})/2$. Clearly, the tubular structure is resulting from chirality through K_n^*. Substituting Eqs. 9 and 10 into Eq. 5, we obtain the minimum elastic free energy per unit area of the tubule as

$$G_{\text{tubule}}^{\min} = -K_n^{*2}/(8\overline{K}_n). \quad [11]$$

We now consider the elastic free energy for a helical ribbon, for which we must include the effect of the ribbon edges. By cutting a parallel strip out of a tubule along a constant helical pitch angle ψ, we may construct a helical ribbon surface as shown in Fig. 1*a*. We assume that the helical strip is cut parallel to the direction of $\hat{\mathbf{c}}$ ($\psi = \beta$) (11, 12) and will determine the optimal value of pitch angle by minimizing the resulting free energy. Removal of the helical strip exposes two helical edges. As a result, while the free energy per unit area of the remaining ribbon remains the same, an additional elastic free energy term associated with the newly exposed edges must be included. Since any curve can be completely specified except for its location by the curvature κ and torsion τ, the elastic free energy per unit length, g_{curve}, due to a small deformation of a curve can be generally expanded (18),

$$g_{\text{curve}} = \frac{\lambda_\kappa}{2}(\kappa - \kappa_0)^2 + \frac{\lambda_\tau}{2}(\tau - \tau_0)^2 + g_0, \quad [12]$$

where λ_κ and λ_τ are elastic moduli for the curvature and torsion and κ_0 and τ_0 are the spontaneous curvature and torsion of the curve, respectively. g_0 [$= g_{\text{curve}}(\kappa_0, \tau_0)$] is the free energy per unit length of a curved edge having the spontaneous curvature and torsion. We have found that inclusion of the edge curvature term results in a change in pitch angle as a function of ribbon width. Since this did not occur experimentally in our system, we regard the magnitude of the curvature term as negligible in contrast to the torsion term. Thus the effect of exposing two edges to the helical ribbon of width w can be accounted for by an extra edge energy per unit area,

$$G_{\text{edge}} = \left[\frac{\Lambda_n}{2}(\tau - \tau_n^0)^2 + g_0\right]\frac{2l}{lw} = \frac{\Lambda_n}{w}(\tau - \tau_n^0)^2 + \frac{2g_0}{w}, \quad [13]$$

where l, Λ_n, $\tau(= \cos\psi \sin\psi/\rho)$ (10), and τ_n^0 are the total length, torsional rigidity, torsion, and spontaneous torsion of a helical ribbon edge, respectively. Then the overall free energy per unit area of the helical ribbon is given by

$$G_{\text{helix}}(\rho, \psi; w) = G_{\text{tubule}}(\rho, \psi) + G_{\text{edge}}(\rho, \psi; w). \quad [14]$$

The geometrical form of the helical ribbon of width w having lowest free energy is found using the conditions,

$$\frac{\partial G_{\text{helix}}}{\partial \rho} = \frac{\partial G_{\text{helix}}}{\partial \psi} = 0. \quad [15]$$

These yield the analytical expressions for the pitch angle ψ and radius $\rho_n(w)$ of an n-bilayer helical ribbon:

$$\tan^4\psi = K_n^{cc}/K_n^{pp}. \quad [16]$$

$$\rho_n(w) = \frac{2w(\overline{K}_n/K_n^*) + (\Lambda_n/K_n^*)}{w + 2\tau_n^0(\Lambda_n/K_n^*)}\sin 2\psi$$

$$= \rho_n^0 + \frac{w(\rho_n^{\text{tubule}} - \rho_n^0)}{w + 2\tau_n^0(\Lambda_n/K_n^*)}, \quad [17]$$

where $\rho_n^0 = \sin\psi\cos\psi/\tau_n^0$ is the radius in the limit of $w \to 0$. Thus, we have obtained the interesting result that regardless of the edges, the optimal pitch angle is equal to the molecular phase angle of the cylindrically grown tubule having a minimum elastic free energy $G_{\text{tubule}}^{\min}$. The pitch angle is also entirely independent of other properties of the ribbon such as the width w and elastic moduli K_n^{cp}, K_n^*, Λ_n, and τ_n^0. For an isotropic bilayer ($K_n^{cc} = K_n^{pp}$), the pitch angle is 45°, identical to Helfrich and Prost's results (11). $\rho_n(w)$ increases with w, provided that $4\overline{K}_n\tau_n^0 > K_n^*$. If this inequality is reversed, $\rho_n(w)$ decreases with w. In the present case, we found experimentally that the former condition applies. In Fig. 7, we plot $\rho_n(w)$ according to Eq. 17. By analyzing experimental data on ρ versus w, one can determine the spontaneous torsion τ_n^0, and the relative magnitudes of elastic moduli, $\overline{K}_n/K_n^*$ and Λ_n/K_n^*. It is important to recognize that the ribbon width can only grow until the two edges merge. According to Fig. 1*a*, this occurs when $\delta = P$, or when $w_{\max}(\rho) = 2\pi\rho \sin\psi$. In Fig. 7, we present $w_{\max}(\rho)$ as a dotted straight line. The intersection between $\rho_n(w)$ and this straight line represents the radius, $\rho_n^{\max}$ of a helically grown tubule. This graph shows clearly that the helically grown tubules should have the same radius $\rho_n^{\max}$ for a fixed n. Note also that the asymptotic value for $\rho_n(w)$ in the limit of $w \to \infty$ is equal to ρ_n^{tubule}, the radius of cylindrically grown tubules.

By inserting the expressions for the pitch angle Eq. 16 and the radius Eq. 17 into Eq. 14, one obtains the dependence of the optimal elastic energy per unit area on the width of a helical ribbon as

$$G_{\text{helix}}^{\min}(w) = -\frac{K_n^{*2}}{8\overline{K}_n} + \frac{\Lambda_n(K_n^* - 4\overline{K}_n\tau_n^0)^2}{8\overline{K}_n(2\overline{K}_n w + \Lambda_n)} + \frac{2g_0}{w}$$

$$= G_{\text{tubule}}^{\min}\{1 - [\rho_n^{\text{tubule}}/\rho_n(w) - 1]^2\} + G_{\text{edge}}. \quad [18]$$

For a positive g_0, $G_{\text{helix}}^{\min}$ decreases monotonically with w toward the value corresponding to $w = w_{\max}$, i.e., toward

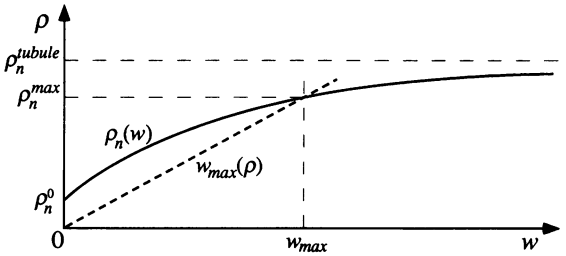

FIG. 7. Theoretical form of radius versus width of the helical ribbon. Solid line represents $\rho_n(w)$ in Eq. 17 and dotted line represents $w_{\max}(\rho)$. The intersection of these two lines determines $\rho_n^{\max}$.

$G^{min}_{helix}(w_{max})$. At w_{max}, however, the ribbon edges merge and G_{edge} disappears. As a result, G^{min}_{helix} drops to a value that is still higher than G^{min}_{tubule} by the amount of $\Delta G = |G^{min}_{tubule}|(\rho_n^{tubule}/\rho_n^{max}-1)^2$. Hence, the helically grown tubule can achieve a lower energy by expanding to a larger radius ρ_n^{tubule}. Indeed, we observed fracture of the tubules consistent with this result. Now we speculate why cylindrically grown tubules do not form. We envision two possible initial configurations for a direct formation of a tubule; the cylindrical growth of a circular strip or circular growth of a straight strip both having a cylindrical curvature of $1/\rho_n^{tubule}$. Since the width of these initial structures is small, edge energies dominate over surface terms. For either of these starting structures, edge energies per unit area are higher than that of a helix with spontaneous torsion by the amount $\Lambda_n(\tau_n^0)^2/w$. Thus initial helices are energetically advantageous relative to cylindrical initial structures. Once a helix is formed, further decrease in energy with w according to Eq. **18** drives the subsequent lateral growth of the helical ribbon to the tubule as was observed experimentally. In principle, alteration of the edge energy, with suitable chemical species in bile, should provide control of the kinetics of this pathway.

So far we have analyzed ribbons of a fixed number of bilayers, n. Let us now discuss the consequences of having different values of n. In that case, the elastic properties of multilamellar ribbons will depend strongly on interlayer interactions, and the elastic moduli will have a spectrum of discrete values depending on the integer number n. The n dependence of the pitch angle will be determined by the ratio K_n^{cc}/K_n^{pp}. If the two bending moduli, K_n^{cc} and K_n^{pp}, have the same n dependence, the pitch angle will be independent of n. Similarly, τ_n^0, $\bar{K}_n/K_n^*$ and Λ_n/K_n^* will determine the n dependence of $\rho_n(w)$ given by Eq. **17**.

Comparison of Theory with Experimental Observations. As can be seen in Figs. 4–6, pitch angles of the helical ribbons were constant and independent of ρ and w, thus confirming that the pitch angle is determined by the ratio of the two elastic moduli as predicted by Eq. **16**. Since pitch angles were observed to be independent of ribbon thickness, the two moduli K_n^{cc} and K_n^{pp} must have the same dependence on n. From the two distinctive pitch angles, we infer that the two kinds of helices have different elastic properties. The calculated ratios K_n^{cc}/K_n^{pp} are 3.4 and 1.5×10^{-3} for the high pitch angle of 53.7° and low pitch angle of 11.1°, respectively. The low pitch helices appear to be composed of hydrated bilayers of cholesterol since the pitch angles were independent of lecithin species, direct transitions of a fractured tubule into a plate-like crystal were observed, and the 11.1 ± 0.5° pitch angle matches the 79.15° (= 90° − 10.85°) edge angle of ChM plates (3). The high pitch helices may be composed of anhydrous cholesterol bilayers. Clearly, it is desirable to obtain further chemical and x-ray data to conclusively establish the composition of both high and low pitch helices.

We have also measured ρ versus w of the helical ribbons and qualitatively observed the corresponding ribbon thickness. These preliminary observations suggest that the data may be grouped into a sequence of curves, as shown in Fig. 8, whose asymptotic radius ρ_n^{tubule} appears to increase monotonically with n. We suggest that the data shown in Fig. 8 may correspond to lamellae having small values of n. Further measurements of thickness are clearly needed. We note that Yager and coworkers (7, 8) have observed helically grown tubules of pure lecithin of constant radius. These findings also point out the importance of future studies of the dependence of the elastic properties on layer thickness.

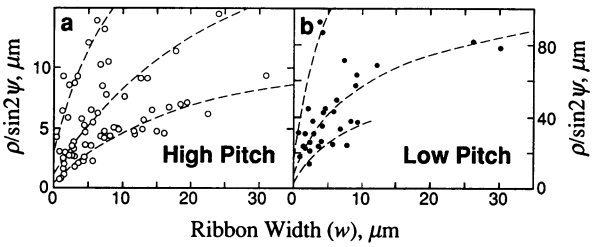

FIG. 8. Radius versus width of helical ribbons for high (*a*) and low (*b*) pitch helices. Possible subgroups having different thicknesses are indicated by dotted lines.

CONCLUSION

Helical ribbon structures are metastable intermediates in the formation of ChMs from model bile. We have analyzed these helical structures using an elastic free energy appropriate for multilamellar bilayers of tilted chiral amphiphiles and obtained a quantitative description of the observed pitch angles and dependence of helix radius on ribbon width. Furthermore, this elastic free energy provides a qualitative understanding of the formation, relative stability, and even the fracture of these intermediates. Our experiments demonstrate that the evolution of these structures is sensitive to the chemical structure of the lecithin component of bile. If these pathways, involving helical intermediates, should prove to be physiologically important, it may be possible to inhibit cholesterol crystallization and associated gallstone formation by controlling the edge energy and, hence, the kinetics of these intermediates.

We acknowledge with thanks valuable suggestions by Profs. M. C. Carey, P. Yager, and W. Helfrich, and the able assistance of Ms. A. Jackson in sample preparation. This work was supported in part by National Science Foundation Materials Research Laboratory Grant DMR 90-22933, the Veterans Affairs Medical Research Fund, and National Institutes of Health Grants DK 36588 and DK 34854.

1. Donovan, J. M. & Carey, M. C. (1991) *Gastroenterol. Clin. North Am.* **20**, 47–56.
2. Konikoff, F. M., Chung, D. S., Donovan, J. M., Small, D. M. & Carey, M. C. (1992) *J. Clin. Invest.* **90**, 1155–1160.
3. Loomis, C. R., Shipley, G. G. & Small, D. M. (1979) *J. Lipid Res.* **20**, 525–535.
4. Tachibana, T. & Kambara, H. (1969) *Bull. Chem. Soc. Jpn.* **42**, 3422–3424.
5. Pfannemüller, B. & Welte, W. (1985) *Chem. Phys. Lipids* **37**, 227–240.
6. Nakashima, N., Asakuma, S. & Kunitake, T. (1985) *J. Am. Chem. Soc.* **107**, 509–510.
7. Georger, J. H., Singh, A., Price, R. R., Schnur, J. M., Yager, P. & Schoen, P. E. (1987) *J. Am. Chem. Soc.* **109**, 6169–6175.
8. Chappell, J. S. & Yager, P. (1991) *Biophys. J.* **60**, 952–965.
9. Servuss, R. M. (1988) *Chem. Phys. Lipids* **46**, 37–41.
10. Helfrich, W. (1986) *J. Chem. Phys.* **85**, 1085–1087.
11. Helfrich, W. & Prost, J. (1988) *Phys. Rev. A* **38**, 3065–3068.
12. Ou-Yang, Z.-c. & Liu, J. (1990) *Phys. Rev. Lett.* **65**, 1679–1682.
13. Carey, M. C. & Small, D. M. (1978) *J. Clin. Invest.* **61**, 998–1026.
14. de Gennes, P.-G. (1974) *The Physics of Liquid Crystals* (Oxford Univ. Press, London).
15. Dahl, I. & Lagerwall, S. T. (1984) *Ferroelectrics* **58**, 215–243.
16. Szleifer, I., Kramer, D., Ben-Shaul, A., Gelbart, W. M. & Safran, S. A. (1990) *J. Chem. Phys.* **92**, 6800–6817.
17. Fischer, T. M. (1992) *Biophys. J.* **63**, 1328–1335.
18. Bugl, P. & Fujita, S. (1969) *J. Chem. Phys.* **50**, 3137–3142.